AIAA Atmospheric Flight Mechanics Conference and Exhibit
18 - 21 August 2008, Honolulu, Hawaii

AIAA 2008-6883

Computational Comparisons of the Interaction of a Lateral Jet on a Supersonic Generic Missile

Patrick Gnemmi*
French-German Research Institute of Saint-Louis (ISL), F-68301 Saint-Louis Cedex, France

Reza Adeli† and José Longo‡
German Aerospace Center (DLR), Institute of Aerodynamics and Flow Technology, Lilienthalplatz 7, G-38108 Braunschweig, Germany

The paper deals with the comparison of computations made at DLR and ISL on the interaction between a lateral jet issuing from a generic missile body and the oncoming supersonic cross-flow. Steady-state numerical simulations are carried out by 3D, viscous, turbulent, Reynolds-Averaged Navier-Stokes codes; at DLR, a hybrid mesh is used for the TAU calculation, whereas at ISL a hexahedral mesh is used for the CFX computation. Experimental data acquired in the DLR wind tunnel TMK in Cologne act as references for the computations. Calculations are made for a cross-flow Mach number of 2.8, for angles of attack of -5, 0 and 10 degrees and for a jet ejection pressure ratio of 100. The test model is a cone-cylinder-flare body with a side-jet nozzle located in the cylindrical part, representing a simple generic high-speed missile configuration. Surface pressure measurements were carried out in order to validate the corresponding computations. The agreement between the computations and the experiments in terms of pressure distribution is obtained with a high degree of accuracy by the codes, in spite of some small discrepancies.

Nomenclature

Cp	=	pressure coefficient
D	=	diameter of the missile model, [mm]
X/D	=	normalized abscissa
φ	=	azimuth angle, [°]
α	=	angle of attack, [°]
R_{OJ}	=	ratio of the jet total pressure divided by the wind-tunnel free-stream static pressure
$y+$	=	normalized distance

I. Introduction

During the homing phase of an interceptor missile, a short response time for its control is mandatory. The use of lateral jets for the missile control offers considerable advantages over conventional surface control methods, in particular as far as the agility and maneuverability of the vehicle are concerned.[1] The main reasons are shorter response times and the fact that the lateral jet control is effective even at a high altitude or low speeds at which dynamic pressures are low. However, a transverse jet issuing from a missile body into a supersonic external flow creates a complex flow field that influences the control efficiency.

In case the jet thruster is switched on, the gases blow out of the thruster and cause an interference with the cross-flow around the missile. The complex flow field developed by the interaction of the laterally blowing gas jet with the supersonic cross-flow is sketched in figure 1. The resulting jet plume is deflected and acts as a massive obstacle

* Dr, Senior Scientist, Aerodynamics and External Ballistics Department, patrick.gnemmi@isl.eu, Senior Member AIAA.
† Dr.-Ing., Scientist, Spacecraft Department, radeli@hotmail.de.
‡ Dr.-Ing., Head, Spacecraft Department, jose.longo@dlr.de, Senior Member AIAA.

located on the surface of the missile. Thus, a strong bow shock is formed in the supersonic flow in front of the jet obstacle. A separation zone develops upstream from the jet, due to the boundary layer separation forming a forward-facing separation shock.[2] In this separation zone, the pressure acting on the body surface becomes higher than the static cross-flow pressure, whereas it decreases in the recirculation zone formed downstream from the lateral jet. As a consequence, the resulting forces acting on the missile are influenced by the interaction of the jet flow with the cross-flow. Indeed, while for some specific orientations and flow conditions, the interaction effects have been found to amplify the lateral force of the jet, under certain other flow conditions and for other orientations, the control jets may cause adverse effects like a deamplification of the thrust. Finally, for a given missile design, the general question to be addressed concerns the amplitude of these resulting forces in order to quantify the efficiency of the side-jet control system.

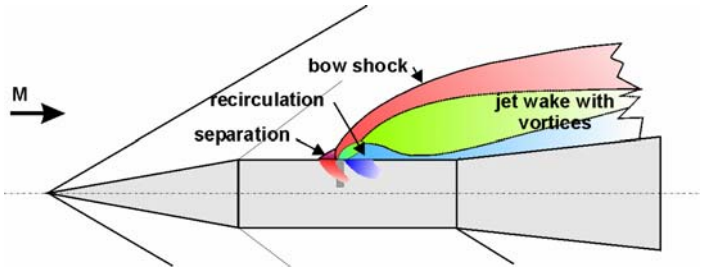

Fig. 1 Interaction of a lateral jet with a supersonic cross-flow

To gain a better understanding of the phenomena that occur with missiles or reentry vehicles using reaction control systems, experimental and numerical investigations of the interaction between a non-reactive, perfect gas jet control system and an external ideal gas flow are conducted for a generic vehicle at DLR and ISL. These have led to the creation of a comprehensive data base regarding mainly the pressure distribution on a high-speed missile body and its dependence on various parameters (Reynolds number of the cross-flow, angle of attack, jet-exit pressure and species of the ejected gas).[3-5] The validation of the computations has been demonstrated independently on the same generic vehicle,[6-8] and the goal of the present paper is to compare in detail the satisfactory results obtained for one missile velocity at 3 angles of attack and for one jet-ejection ratio.

II. Experimental Facility and Instrumentation

The experiments were conducted at the trisonic wind tunnel (TMK) in Cologne-Porz about 10 years ago.[3]

A. TMK Wind Tunnel

The TMK wind tunnel is an intermittent trisonic blow-down tunnel with a closed test section of 0.6 m × 0.6 m. The maximum blow duration is 60 s and the Mach number ranges from 0.5 to 4.5 (5.7 with an ejector). The Mach number can be varied by using an adjustable diffuser and a flexible nozzle. A test section with all-round perforated walls with a variable slotting ratio is available for transonic testing. The maximum total pressure is 26 bar and the total temperature ranges from the ambient temperature to 550 K. The Reynolds number based on a 1 m length ranges from $6 \bullet 10^6$ up to $80 \bullet 10^6$. Special equipments are used for cold-jet simulations.

B. Generic Missile Model

The test model used for the investigations is a circular cross-section body (diameter $D = 40$ mm) which is assumed to be representative of a high-speed missile of a generic shape (Fig. 2). It consists of a cone-shaped nose, a cylindrical body and an adjacent flared afterbody, which in turn is connected to a cylindrical aft extension. A circular, sonic side-jet nozzle of 4 mm ($0.1\,D$) in diameter is located on the cylindrical mid-section at an azimuth of $\varphi = 180°$ and a position of $X = 4.3\,D$ downstream from the model tip. The jet axis is perpendicular to the longitudinal axis of the model. The test model is equipped with series of static-pressure orifices for pressure measurements on the model surface. About 150 orifices are located in four cross-sections

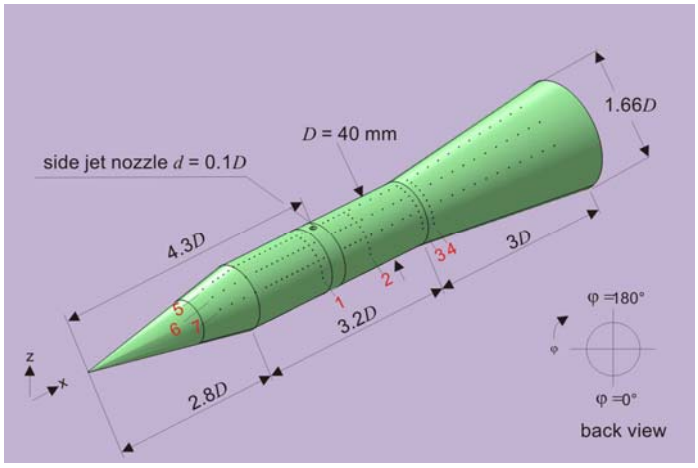

Fig. 2 Cone-cylinder-flare model with side-jet nozzle

(numbered from 1 to 4) and three longitudinal ones (5 to 7). Table I shows the precise location of the sections.

C. Test Conditions

The Mach number of the cross-flow is 2.8, the static temperature and the static pressure are 108.96 K and 20793.2 Pa, respectively. The Reynolds number based on the test-model diameter is $2.06 \bullet 10^6$. Angles of attack (α) of -5, 0 and 10° are considered for the present investigations. The ejection pressure ratio R_{0J}, which is the total jet pressure divided by the wind-tunnel free-stream static pressure, defines the jet strength; it is 100 in the present study.

Table I Location of sections

section	*X/D*	section	φ
1	4.0	5	180°
2	4.9	6	150°
3	5.9	7	120°
4	6.1		

D. Pressure Measurements

The model is equipped with series of static-pressure orifices, as described in Section II.B. The static-pressure survey of the test model surface is carried out by means of a Series 8400 pressure-scanning and data-acquisition system from Pressure Systems Inc. (PSI). This system is composed of Electronically Scanned Pressure (ESP) modules, a Scanner Interface, a Remote Processor with the Pressure Calibration Unit (PCU) and the main system processor comprising the Scanner Digitizer Unit (SDU). The PSI 8400 System is embedded in the general data acquisition system of the wind-tunnel facility. The overall error on the determination of the pressure coefficient is dominated by the uncertainty regarding the true cross-flow conditions; it turned out to be lower than ± 0.005.[8]

III. Numerical Methods

Steady-state numerical simulations are conducted by 3D, viscous, turbulent, Reynolds-Averaged Navier-Stokes codes. At DLR computations are made by running the DLR TAU code which uses a hybrid mesh, whereas at ISL they are carried out with the commercial CFX-10[*] code using a hexahedral mesh.

A. TAU Code

The DLR-developed TAU code[9] is used to solve the Reynolds-Averaged Navier-Stokes equations. The discretization of space and time is performed independently. The space discretization is an unstructured, finite-volume approximation, while the time discretization is achieved using an explicit Runge-Kutta method. The grid can be made up of tetrahedrons, prisms, pyramids and hexagons. The flow is calculated using a dual grid generated by preprocessing modules. The discretization of the convective terms (Euler terms) is achieved using centralized or upwind methods, while the viscous flow is discretized using a centralized method. For more detailed information, see Refs. 9 and 10.

1. Grid Generation

The numerical simulations require a geometrical discretization of the region of interest. A 3D grid is generated using the CENTAUR program.[11] That program uses CAD-data in the form of IGS/IGES files. With this program the boundary conditions for the differential equations can be defined for each panel. CENTAUR provides structured as well as unstructured 3D hybrid grids for numerical analysis consisting of cells of varying shapes.

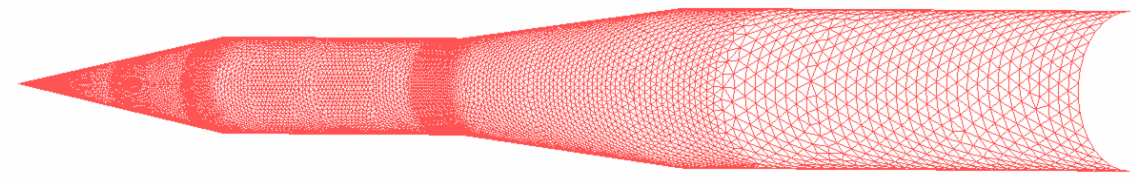

Fig. 3 Test-model grid generated for TAU computations

Since the flight vehicle is axisymmetric, the geometry is reduced to a cylinder. Several grids are generated around this geometry. Geometric sources in the shape of hollow cylinders are defined at the transitions from the nose cone to the cylindrical body and from the cylindrical body to the flare. The forward parts of these cylinders are refined, thus creating a hybrid grid with a prismatic surface (Fig. 3).

For the flow-field discretization, the height of each successive layer equals that of the previous layer multiplied by a scaling factor of 1.25. The boundary layer fits nicely 16 prismatic cells for the studied supersonic Mach

[*] CFX-10™ is a trademark of ANSYS Canada Ltd.

number. This assertion is based on calculations for the jet-on case of $R_{0J} = 50$ executed with another grid containing approximately the same number of nodes, but twice as many prismatic cells, which delivered the same results for the forces, pressure coefficients and amplification factors (see section on accuracy).[6] Finally, the mesh used for the numerical simulations has 760,000 nodes (Fig. 4). The grid is built in such a way that the y^+ values are near 0.3.

2. Numerical Accuracy

A parametric study under jet-off conditions was conducted to examine the influences of the grid and the turbulence models. The analysis of the pressure-coefficient (*Cp*) distributions shows that the grid convergence is demonstrated and that all the turbulence models provide a good correlation with the experimental data.[6]

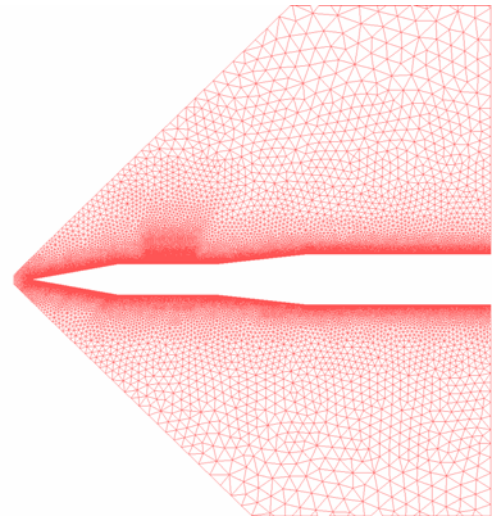

Fig. 4 Grid used for TAU computations, 760,000 nodes

Several grids and various turbulence models were investigated to assess the numerical solutions with respect to numerical errors and physical modelling for the jet-on case. The parametric study was carried out for the $R_{0J} = 50$ case. The detailed analysis of the pressure-coefficient distributions shows a nearly achieved grid convergence, except for some areas of the flow separation. A good correlation of the numerical results with the experimental data is obtained using a fine grid with local adaptations of about 760,000 nodes. This was also verified for the super-fine grid with 2,589,107 nodes. That analysis also shows the sensitivity of the results to the various turbulence models: it turns out that the k-ε model leads to an additional local boundary layer separation upstream from the jet which is not obtained with the k-ω model and the Spalart-Almaras model and which is not shown by the experimental data either.

Finally, the computations presented in the present paper are made by using the fine grid with 760,000 nodes and by using the Spalart-Almaras turbulence model, and the convergence residuals are smaller than 10^{-4}.

B. CFX Code

The fluid solver of the CFX-10 code is based on Reynolds-Averaged Navier-Stokes equations and provides a solution for the three-dimensional, steady-state, compressible and turbulent single-phase fluid flow. A two-equation turbulence model or a Reynolds-stress turbulence model is used to close the equation system for turbulent flows. The code is built on a Finite Volume Method that uses different discretization schemes: from the most robust scheme giving a first-order prediction to the most accurate numerical discretization scheme giving a second-order solution. A convergence criterion ends the computation and allows a stationary converged solution to the problem to be obtained. This criterion is based on the maximum of the current dimensionless residual value for each conservation equation of mass, momentum and energy. The software uses multi-block-structured non-orthogonal grids, unstructured grids or hybrid grids in order to spatially discretize the domain.

1. Grid Generation

The computational domain is reduced to one half of the complete domain, due to the symmetry of the problem. The computation is only focused on the flow around the body, so that the wake of the model is not meshed. The mesh around the body and the mesh of the jet nozzle form a multi-block structured grid of the "H" type. The jet nozzle cylindrical mesh is attached to the main mesh in such a way that the nodes of the jet nozzle exit exactly correspond to the ones on the missile model surface.

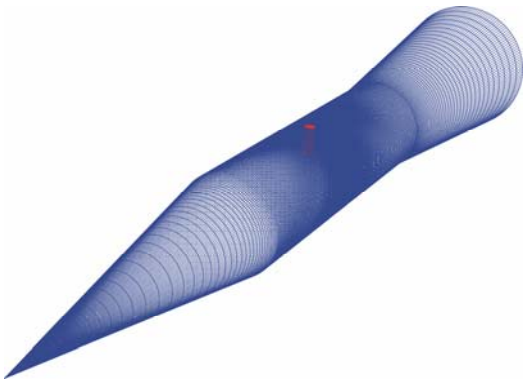

Fig. 5 Test-model grid generated for CFX computations

The computational domain is limited by the surfaces where the boundary conditions are fixed. The missile model is located within a half-cylindrical volume which is itself located within a half-prismatic volume. The surface limits the computational domain to 5 D from the missile symmetry axis. The conical upstream surface is located only at a half-missile diameter (0.5 D) ahead of the missile nose, since the external flow is supersonic. The cone angle is about 45°, which nearly corresponds to the orientation of the jet plume. The conical

downstream surface is located at the end of the missile surface. One end surface of the cylindrical mesh of the vertical jet nozzle is connected to the mesh of the external flow, as mentioned before. The other end surface of the jet nozzle mesh is a perpendicular plane to the jet nozzle axis, where the working conditions are imposed; this plane is located 12 mm inside the missile model.

The optimal performance of turbulence models is achieved by the proper resolution of the boundary layer and the correct spacing of the first point near the wall. The boundary layer is resolved with a minimum of 20 nodes in the direction normal to the wall. The use of the near-wall treatment allows the building of meshes such that $y^+ \leq 100$: several meshes are built with different densities of the node distribution in the boundary layer. The finest mesh is composed of 425 nodes in the longitudinal direction and 85 nodes around the circumference of the model (Fig. 5). 75 nodes in the radial direction are distributed in the external flow mesh. 60 nodes are distributed in the longitudinal direction of the jet nozzle and 41 x 21 nodes are in the jet nozzle section. Finally, the mesh used for the numerical simulations has 2,761,035 nodes (Fig. 6). The distance between a node located on the projectile surface and the first node located in the flow is 1.2 µm. Therefore, the mesh is built in such a way that the y^+ values are lower than 2, allowing the use of the near-wall treatment.

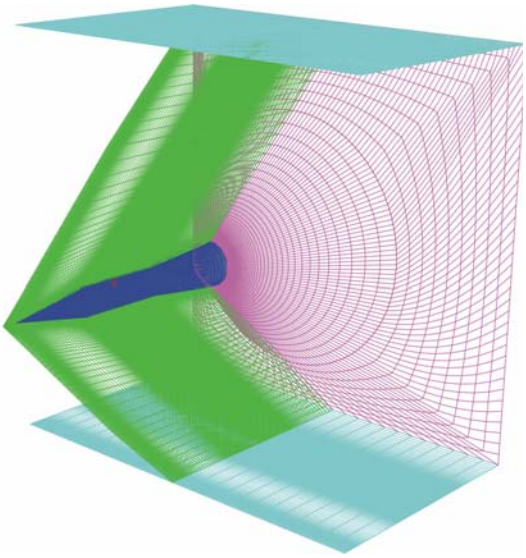

Fig. 6 Grid used for CFX-10 computation, 2,761,035 nodes

2. Numerical Accuracy

A detailed study of different supersonic projectiles and missiles with no jet interaction was conducted in order to examine the influence of turbulence models and grid refinements on numerical results.[12,13] Standard and RNG k-ε turbulence models[14,15] using different near-wall treatments[16,17] were studied. The coupled k-ε / k-ω turbulence models (*BSL* and *SST*) developed by Menter,[18] using the automatic near-wall treatment,[16] were also applied. Reynolds-stress turbulence models designed by Launder-Reece-Rodi[19] and Speziale-Sarkar-Gatski,[20] using the same near-wall treatment as for k-ε turbulence models, were also studied. The flow field around different forebodies at several Mach numbers and angles of attack was computed, including flow separation in some cases. The analysis of the huge amount of computational results makes it possible to conclude that the aerodynamic coefficients are slightly influenced by the choice of a turbulence model based on 2 transport equations (k-ε, k-ε / k-ω) and by the node density in the boundary layer. The accuracy of the prediction of the surface pressure, axial force, normal force and pitching moment coefficients is estimated to be ± 2%. Moreover, the computed global coefficients were compared with the experimental ones: the axial force coefficient and the derivative of the normal force coefficient are overestimated by 2% and 8%, respectively; the derivative of the pitching moment is underestimated by 5%.

Furthermore, a parametric study conducted for the present generic missile under jet-on conditions ($50 \leq R_{0J} \leq 100$) investigated the influences of the grid.[7] The analysis of the pressure-coefficient (Cp) distributions shows that the grid convergence is demonstrated, but the computational mesh must be very fine around the jet exit in the separation region of the boundary layer in order to accurately predict that separation. Taking into account the conclusions of these detailed studies, the accuracy of the prediction of the surface pressure, drag, lift and pitching moment coefficients is estimated to be around ± 2%.

Finally, the computational grid with slightly more than 2.7 million nodes and the *SST* two-equation model of turbulence with the automatic detection and switch from the scalable wall functions to a low-Reynolds-number near-wall formulation are used. The convergence residuals are smaller than 10^{-4} for the present calculations.

IV. Numerical Results and Comparison with Measurements

Numerical simulations are carried out with each code for different angles of attack (α) but only the results for angles of attack of 0, –5 and 10° are presented.

A pair of wake vortices dominates the flow field downstream from the jet exit as can be seen in Fig. 7 for the angle of attack of 10°. The figure shows the surface and three-dimensional streamlines characterizing the interaction between the lateral jet and the cross-flow of the missile model. The streamline colour represents the velocity. The missile model is coloured in pink. It can also be observed that the bow shock introduced by the jet interacts with the vehicle boundary layer ahead of the jet exit. The boundary layer separates and due to the supersonic character of the

flow, a lambda shock takes place and a horseshoe vortex caused by that separation is clearly identified. Other calculations of various flow conditions show an increase in the distance between the bow shock and the jet exit when increasing the jet-ejection pressure and therefore, a size increase of the boundary layer separation region.[6,7] A second separated region downstream from the jet shows the same characteristics as a separation caused by a backward-facing step. Due to the supersonic character of the flow, a recompression shock in this region is necessary to change the direction of the flow.

Figure 8 depicts the detailed flow-field topology in the symmetry plane ($\varphi = 180°$) close to the lateral jet exit for the angle of attack of 0°. The jet creates the obstacle for the cross-flow which produces the bow shock (B). The bow shock is easily discerned when looking at the abrupt change of direction of the streamlines and the decrease of the Mach number from 2.8 to a subsonic level. The high adverse pressure gradient leads to the premature separation of the boundary layer (A) by which the strong bow shock forms a weaker lambda-shock wave structure on the vehicle surface with a lower adverse pressure gradient. A vortex structure is created inside the lambda-shock structure. A second discernible shock structure is the barrel shock (C) which engulfs the over expanded region of the lateral jet plume. The Mach disk (E) terminates this region in the direction of the jet flow and the flow reaccelerates downstream from the Mach disk. This shock-wave system induces a flow separation immediately downstream from the jet exit on the surface of the flight vehicle (D) and leads to the emergence of vortices in the flow field. Figures 7 and 8 complete the sketch of figure 1.

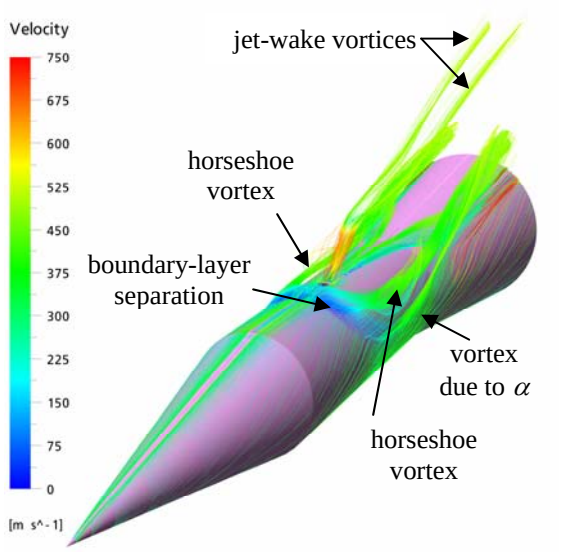

Fig. 7 Structure of the flow field visualized by surface and 3D streamlines, $\alpha = 10°$

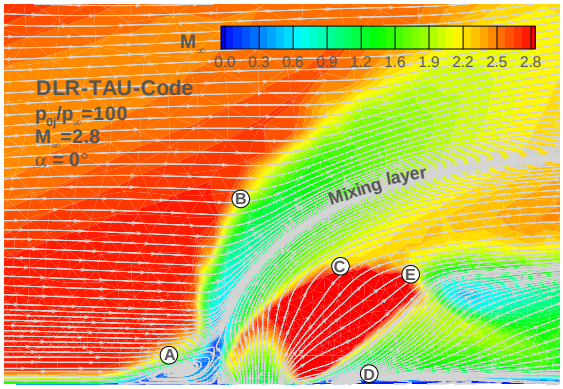

Fig. 8 Structure of the flow field, $\alpha = 0°$

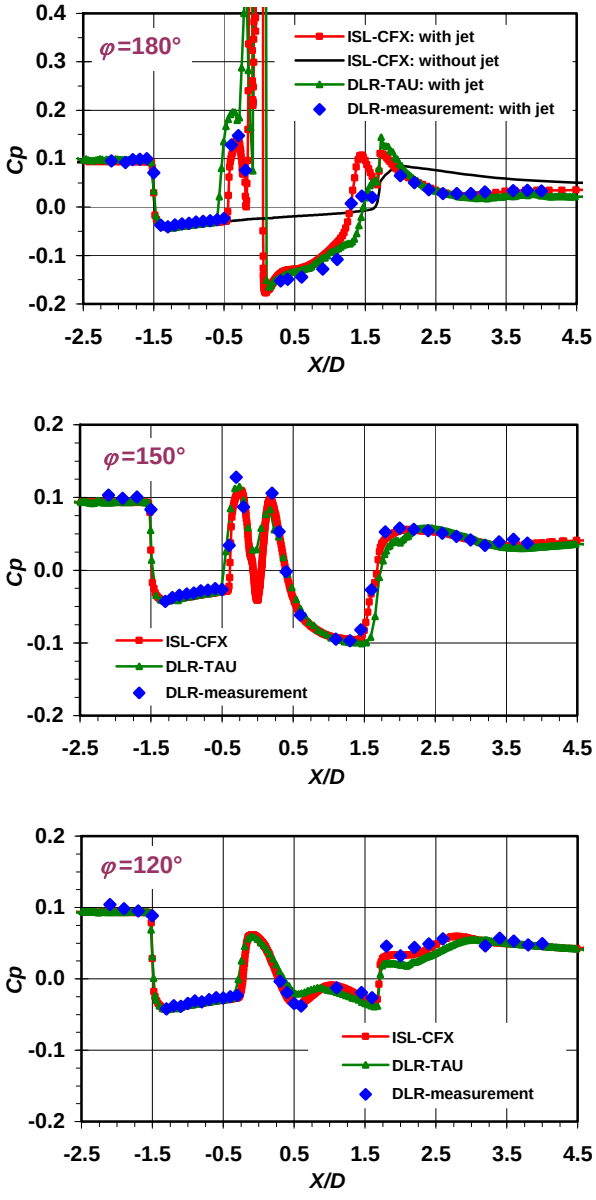

Fig. 9 Comparison of the CFX and TAU computed pressure coefficient with the measured one, $\alpha = 0°$

In the following sections, the computed pressure distributions are compared with the experimental ones on meridians 5 to 7 defined in Fig. 2 and Table I.

A. Angle of Attack of 0°

Figure 9 presents the results for $\varphi = 180°$, $\varphi = 150°$ and $\varphi = 120°$, the test model having no angle of attack. In the upper graph, the pressure coefficient computed on the lower meridian, corresponding to the result without any jet, is also shown. The symbols of the computed results are located at the nodes of the meshes, showing the smoothness of the grid on the model surface. The abscissa $X/D = 0$ corresponds to the location of the vertical axis of the jet nozzle: thus, the jet exit is situated in such a way that $-0.05 \le X/D \le 0.05$. The cross-flow goes from left to right and the jet flow is produced from the bottom upwards.

Both numerical simulations predict the pressure distributions with a very good accuracy, in spite of small discrepancies mainly visible in the symmetry plane ($\varphi = 180°$). The TAU code slightly overestimates the separation region ahead of the jet exit. The CFX code slightly overvalues the reattachment shock near $X/D = 1.1$, whereas both codes correctly predict the recompression shock produced by the flare near $X/D = 1.7$.

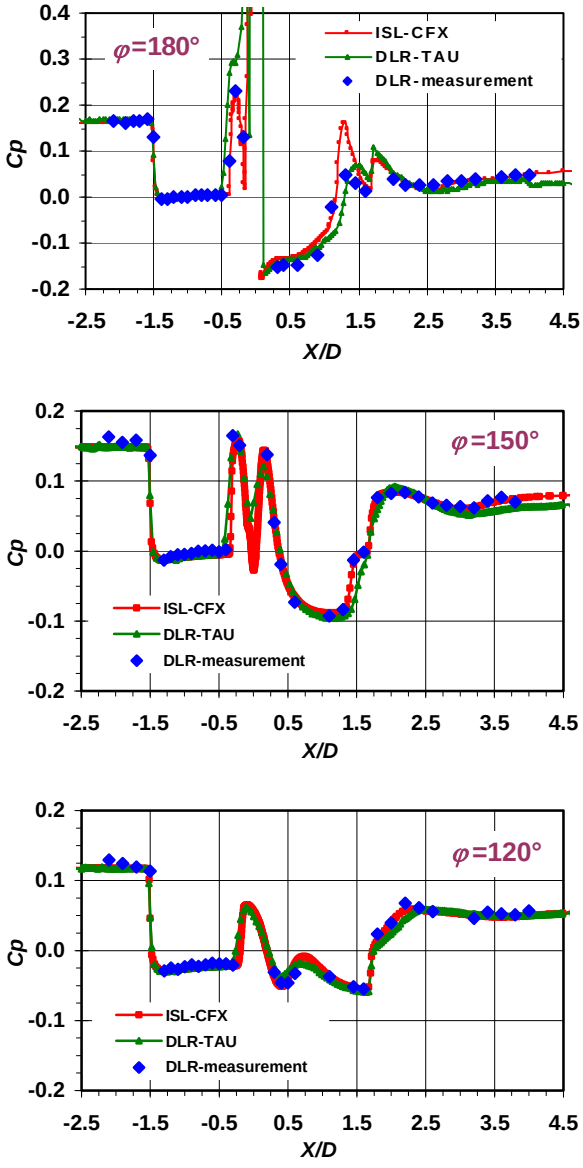

Fig. 10 Comparison of the CFX and TAU computed pressure coefficient with the measured one, $\alpha = -5°$

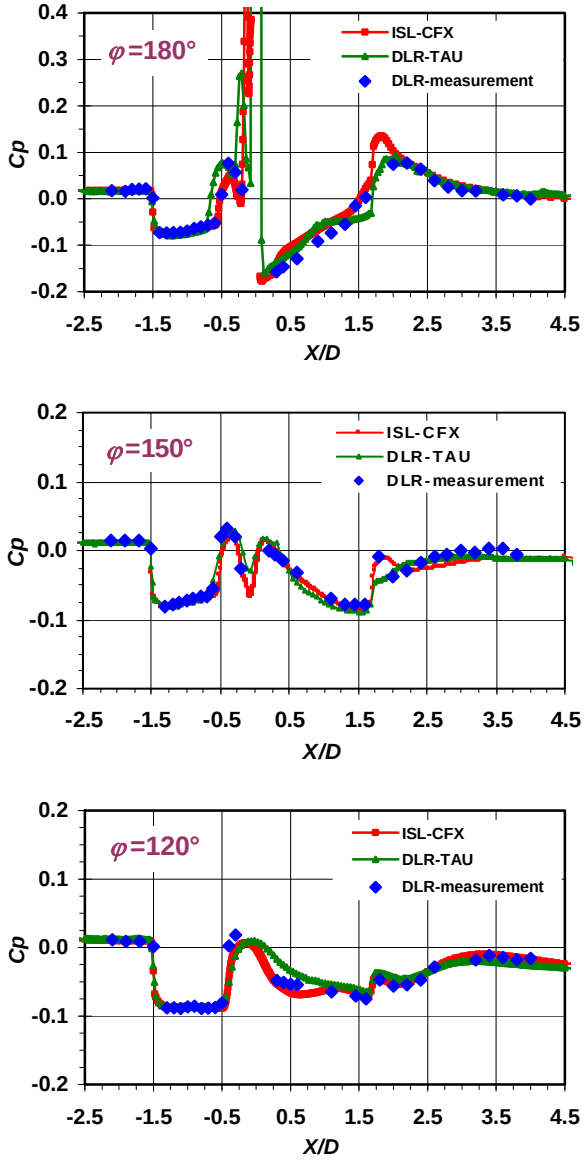

Fig. 11 Comparison of the CFX and TAU computed pressure coefficient with the measured one, $\alpha = 10°$

B. Angle of Attack of –5°

Figure 10 depicts the same kind of results for an angle of attack of –5° of the test model. A negative angle of attack means that the missile model is oriented nose-down in the wind tunnel.

The separation zone of the boundary layer ahead of the jet exit is a little smaller than in the configuration for $\alpha = 0$. The overpressure is consequently higher in that region for $\alpha = -5°$ than for $\alpha = 0°$. The agreement between the computation and the experiment is very satisfactory. The remarks formulated for $\alpha = 0°$ remain valid for that angle of attack: the discrepancies between the computations and the measurements are particularly visible in the symmetry plane ($\varphi = 180°$), in the reattachment shock zone and in the boundary layer separation region.

C. Angle of Attack of 10°

Figure 11 depicts the same kind of results for the angle of attack of 10° of the test model. A positive angle of attack means that the missile model is oriented nose-up in the wind tunnel.

For that configuration the separation region of the boundary layer ahead of the jet is larger than the one obtained for the other angles of attack. The overpressure is lower in that region for $\alpha = 10°$ than for the other angles of attack. The numerical simulation prediction of the pressure distribution is in very good agreement with the measurements. As underlined by the measurements, the reattachment shock is diluted within the recompression shock near $X/D = 1.7$ or it does not exist, which is perfectly predicted by the computation. The discrepancies between the computations remain mainly in the symmetry plane ($\varphi = 180°$), in the reattachment shock zone and in the boundary layer separation region.

V. Conclusion

The experimental investigations of the interaction of a transverse jet with the external flow of a generic missile conducted in the DLR TMK wind tunnel at a Mach number of 2.8 were used for the detailed comparison of the results given by the CFD codes used at ISL and DLR. The missile angle of attack ranged from –5° to 10° and the jet-flow conditions were characterized by a jet-ejection pressure ratio of 100. The test model is a cone-cylinder-flare body with a side-jet nozzle located on the cylindrical part, representing a simple generic high-speed missile configuration. The ratio of the jet-nozzle section to the mean missile cross-section is 1:100.

The computations and the pressure measurements made on the missile model allow a very good understanding of the complex flow field generated by the interaction process. Numerical simulations modelling the experiments were conducted at ISL with the CFX-10 commercial code and at DLR with the TAU code; the *SST* and the Spalart-Almaras turbulence models, particularly recommended for the computation of the flow separation encountered in our application, were respectively used to solve the turbulent regime of the flow.

Both numerical solutions obtained here show a very good correlation with the pressure-distribution measurements from wind-tunnel experiments. Some small discrepancies between the codes mainly occurred in the symmetry plane where the TAU code slightly overestimates the separation region ahead of the jet exit, whereas the CFX code slightly overvalues the reattachment shock. However, the essential details about the dominant features of the interaction process between the lateral jet-flow and the cross-flow, such as shock-induced boundary-layer separation, Mach disk, recompression shock and wake and horseshoe vortices are well captured by both numerical simulations.

Acknowledgments

The authors would like to acknowledge the support of the German Ministry of Defense for that work and wish to express their thanks to H. Esch and H. Emunds for their contribution to the realization of the experiments.

References

[1]Champigny, P., and Lacau, R.G., "Lateral Jet Control for Tactical Missiles," *Special Course on Missile Aerodynamics*, AGARD-FDP Von Karman Institute, Brussels, Belgium, June 6-10, 1994, pp. 3.1-3.57.

[2]Zukoski, E.E., and Spaid, F.W., "Secondary Injection of Gases into a Supersonic Flow," *AIAA Journal*, Vol. 2, No. 10, 1964, pp. 1689-1696.

[3]Esch, H., "Druckverteilungsmessung an einem Flugkörperrumpf im Überschall - Messdaten," DLR Report IB-39113-97C03, 1997.

[4]Esch, H., "Querschubstrahl-Interferenzen an einem Flugkörperrumpf im Überschall bei unterschiedlichen Ausblasemedien," DLR Report IB-39113-99C27, 1999.

[5]Schäfer, H. J., Augenstein, E., Esch, H., and Emunds, H., "Experimental Investigation of Tranverse Jet Interaction on a Missile Body using Laser Velocimetry and Flow Visualization", *19th International Congress on Instrumentation in Aerospace Simulation Facilities* (ICIASF'2001 Record, IEEE Publ. 01CH37215), Cleveland/OH, USA, August 27-30, 2001, pp. 295-301.

[6]Adeli, R., Longo, J.M.A., and Emunds, H., "Flow Fields Study of a Supersonic Jet Exiting into a Supersonic Stream," *Notes on Numerical Fluid Mechanics and Multidisciplinary Design*, Vol. 92. *New Results in Numerical and Experimental Fluid Mechanics V*, Springer 2006, pp. 160-167.

[7]Gnemmi, P., Schäfer, H. J., "Experimental and Numerical Investigations of a Transverse Jet Interaction on a Missile Body," *43rd AIAA Aerospace Sciences Meeting and Exhibit*, Reno/NV, USA, January 10-13, 2005.

[8]Gnemmi, P., Eichhorn, A., Emunds, H., Esch, H., Gülhan, A., Leopold, F., and Schäfer, H. J., "Experimental and Computational Study of the Interaction between a Lateral Jet and the Supersonic External Flow on a Generic Missile Body," *NATO RTO-AMP-AVT-135 Symposium on Innovative Missile Systems*, Amsterdam, The Netherlands, May 15-18, 2006.

[9]Technical Report Technical Documentation of the DLR-TAU-Code, version: 2002.1.0, 2002.

[10]Mack, A., Hannemann, V., "Validation of the Unstructured DLR-TAU-Code for Hypersonic Flow; *32nd AIAA Fluid Dynamics Conference*, AIAA Paper 2002-31111, 2002.

[11]CENTAUR V5.0 Online Documentation, http:// www.centaursoft.com, 2004.

[12]Gnemmi, P., "Influence des modèles de turbulence sur la prévision de l'aérothermodynamique d'un projectile de 155 mm," ISL Report CR/RV 458/2002, 2002.

[13]Gnemmi, P., "Influence des modèles de turbulence sur la prévision de l'aérothermodynamique de l'avant-corps d'engins génériques d'un missile," ISL Report CR/RV 475/2002, 2002.

[14]Launder, B.E., and Spalding, D.B., "The Numerical Computation of Turbulent Flows," *Comp. Meth. Appl. Mech. Eng.*, Vol. 3, 1974, pp. 269-289.

[15]Yakhot, V., Orszag, S.A., Tangham, S., Gatski, T.B., and Speziale, C.G., "Development of Turbulence Models for Shear Flows by a Double Expansion Technique," *Physics of Fluids*, Vol. 4, No. 7, 1992, pp. 1510-1520.

[16]Grotjans, H., and Menter, F.R. "Wall Functions for General Application CFD Codes", *Computational Fluids Dynamics'98*, edited by K.D. Papailiou, Vol. 1, Part 2, John Wiley & Sons, Chichester, U.K., 1998, pp. 1112-1117.

[17]Huang, P.G., Bradshaw, P., and Coakley, T.J., "Skin Friction and Velocity Profile Family for Compressible Turbulent Boundary Layer," *AIAA Journal*, Vol. 31, No. 9, 1993, pp. 1600-1604.

[18]Menter, F.R., "Two-Equation Eddy-Viscosity Turbulence Models for Engineering Application," *AIAA Journal*, Vol. 32, No. 8, 1994, pp. 1598-1605.

[19]Launder, B.E., Reece, G.J., and Rodi, W., "Progress in the Development of a Reynolds-Stress Turbulence Closure," *Journal of Fluid Mechanics*, Vol. 68, Part 3, April 1975, pp. 537-566.

[20]Speziale, C.G., Sarkar, S., and Gatski, T.B., "Modelling the Pressure-Strain Correlation of Turbulence: an Invariant Dynamical Systems Approach," *Journal of Fluid Mechanics*, Vol. 227, June 1991, pp. 245-272.